Device

Article

Washable textile biosensors enabled by nanostructured oxides with fast ion diffusion

Graphical abstract

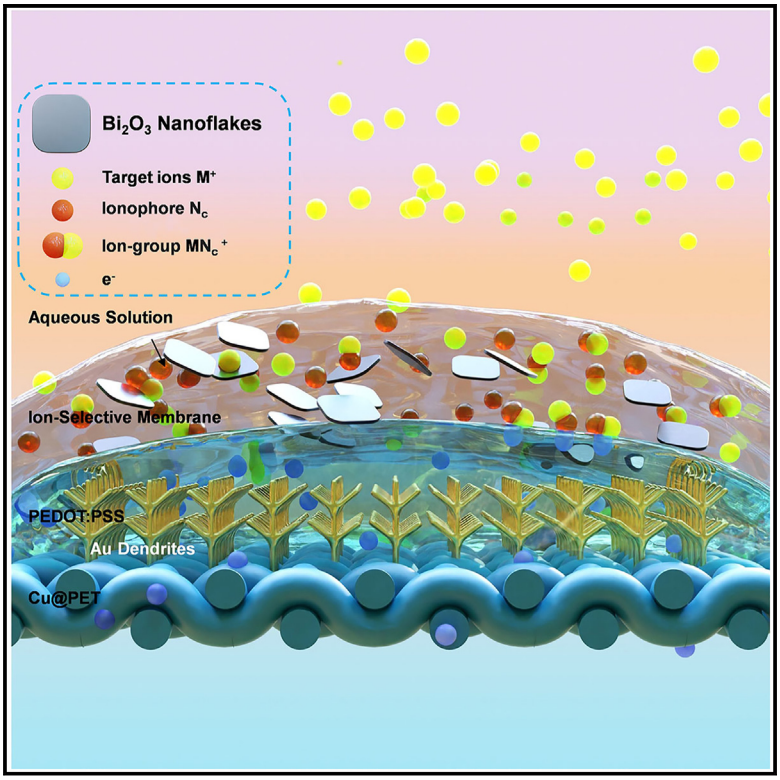

Highlights

- Textile-based sensor washability enhanced by β-Bi_2O_3 nanoflakes
- β-Bi_2O_3 nanoflakes with fast ion diffusion provide 58.70 mV/dec sensing ability
- The β-Bi_2O_3 treatment is resistant against washing with water and laundry detergent
- An epidermal sweat sensor is created using the β-Bi_2O_3-nanoflake-based textile

Authors

Yuqing Shi, Kemeng Zhou, Xiaohao Ma, ..., Qiyao Huang, Zijian Zheng, Yuanjing Lin

Correspondence

zijian.zheng@polyu.edu.hk (Z.Z.), linyj2020@sustech.edu.cn (Y.L.)

In brief

Textile-based biosensors have been functionalized with rational-engineered nanostructured β-Bi_2O_3 nanoflakes. Sodium ion (Na^+) sensors are critical in monitoring various physiological parameters, as sodium levels in bodily fluids can indicate hydration status, kidney function, and electrolyte balance. In this work, Na^+ sensors were developed to address the challenges of wearable applications that require both high sensitivity and durability. The β-Bi_2O_3 nanoflakes electrochemically decorated onto the ion-selective layers provide hydrophobicity and moisture stability without introducing large impedance due to their fast ion conductivity. The Na^+ sensors deliver a sensitivity of 58.70 mV/dec and a retention of over 90% after 20 washing cycles.

3 **Develop**
Prototype with demonstrated applications in relevant environment

Shi et al., 2024, Device 2, 100503
November 15, 2024
https://doi.org/10.1016/j.device.2024.100503

CellPress

Please cite this article in press as: Shi et al., Washable textile biosensors enabled by nanostructured oxides with fast ion diffusion, Device (2024), https://doi.org/10.1016/j.device.2024.100503

Device

CellPress
OPEN ACCESS

Article

Washable textile biosensors enabled by nanostructured oxides with fast ion diffusion

Yuqing Shi,[1,2] Kemeng Zhou,[1] Xiaohao Ma,[1,2] Liting Huang,[1] Xinmeng Hu,[3] Pengwei Wang,[2] Yaokang Zhang,[2] Fan Chen,[5] Mingli Huang,[1] Jiazhen Wu,[3] Xin He,[3,4] Qiyao Huang,[2,6] Zijian Zheng,[2,5,6,7,*] and Yuanjing Lin[1,8,*]

[1]School of Microelectronics, Southern University of Science and Technology, Shenzhen 518055, China
[2]Laboratory for Advanced Interfacial Materials and Devices, School of Fashion and Textiles, The Hong Kong Polytechnic University, Kowloon, Hong Kong SAR, China
[3]Department of Materials Engineering, Southern University of Science and Technology, Shenzhen 518055, China
[4]School of Chemical Engineering, Sichuan University, Chengdu 610065, China
[5]Department of Applied Biology and Chemical Technology, Faculty of Science, The Hong Kong Polytechnic University, Kowloon, Hong Kong SAR, China
[6]Research Institute for Intelligent Wearable Systems, The Hong Kong Polytechnic University, Kowloon, Hong Kong SAR, China
[7]Research Institute for Smart Energy, The Hong Kong Polytechnic University, Kowloon, Hong Kong SAR, China
[8]Lead contact
*Correspondence: zijian.zheng@polyu.edu.hk (Z.Z.), linyj2020@sustech.edu.cn (Y.L.)
https://doi.org/10.1016/j.device.2024.100503

THE BIGGER PICTURE The integration of electronics into textiles is useful for monitoring health in casual and non-clinical settings. Despite recent advancements in textile-based electronics, there remains the challenge of maintaining their functionality and durability through the wear and tear of prolonged usage, particularly in the washing process. Previous research efforts to realize washable devices mainly rely on bulky encapsulation, e.g., using rigid sealing or impermeable layers of polymers like silicone or epoxy25–27. Although these methods serve well for sensor devices and systems based on relatively robust materials such as metals or carbon, they sacrifice permeability and wearing comfort. Here, we present a textile-based biosensor for epidermal sweat sensing created using β-Bi_2O_3 nanoflakes that is sensitive, breathable, and resilient against washing cycles.

SUMMARY

Textile-based electronics possess comfortable epidermal contact and the potential for wearable healthcare applications such as non-invasive sweat biosensing. However, achieving washable biosensors without sacrificing sensitivity and wearing comfort remains a challenge. Herein, we develop β-Bi_2O_3 nanoflakes, which enable washable textile-based biosensors. The β-Bi_2O_3 nanoflakes with fast ion conductivity possess high moisture stability without introducing large impedance. The incorporation of β-Bi_2O_3 nanoflakes improved the sensitivity and washability of textile ionic sensors for sodium, potassium, and proton sensing, with a performance retention of over 90% after 20 washing cycles. As a demonstration, we created a washable and reusable integrated electronic textile wristband for wireless sweat biomarker analysis. This work showcases the use of nanostructured oxides as a washing-resistive layer and a fast ion conductor to confer washability on textile-based sensing devices.

INTRODUCTION

Textile-based electronics provide the advantages of wearing comfort, flexibility, and light weight for a variety of wearable applications, such as fitness monitoring and healthcare.[1–13] Among the various flexible electronics, textile-based electronics with good moisture permeability have the advantage of easy integration with garments.[14–19] For instance, biosensing arrays have been integrated onto textile platforms for wireless epidermal sweat biomarkers analysis.[20–24] However, one of the challenges lies in achieving washable and reusable electronic textiles (e-textiles), which poses high requirements on the active materials stability and device robustness under the mechanical interferences during the washing process. Previous research efforts to realize washable devices mainly have mainly relied on bulky encapsulation, e.g., using rigid sealing or impermeable layers of polymers like silicone or epoxy.[25–27] Although these methods serve well for sensor devices and systems based on relatively robust materials

Please cite this article in press as: Shi et al., Washable textile biosensors enabled by nanostructured oxides with fast ion diffusion, Device (2024), https://doi.org/10.1016/j.device.2024.100503

such as metals or carbon, they sacrifice permeability and wearing comfort. These methods also lack compatibility with biosensors that require direct contact between sensors and biomarkers, such as for applications in epidermal sweat sensing, especially for highly selective biosensors with multiple layers including bioreceptors, which could easily lose their functionalities with variations in humidity, pH, and temperature.[28–30] Therefore, alternative strategies to achieve biosensors with washability by incorporating protective materials onto the sensing electrodes to enhance their intrinsic stability are needed.

Functional materials with moisture resistance have the potential to construct protective layers on biosensors based on highly sensitive and selective bioreceptors. Among them, Bi_2O_3 has been adopted as the filling material for dental applications because of its chemical and mechanical stability in a liquid environment, high radiopacity, and biocompatibility, ensuring nontoxicity and safety for human tissues.[31–35] However, forming such a dense film would introduce a large impedance, which would hinder ion contact and transfer and could result in decreased sensitivity. Realizing the sensing sensitivity and washability requires structural design and materials engineering of such moisture-resistant oxides with fast ion-conducting capability. Fast ion conductors have been utilized for electrochemical devices that require rapid ion movement, such as in rechargeable batteries and fuel cells.[36–38] β-Bi_2O_3 possesses a distinctive crystal structure and exhibits typical fast ion-conducting properties.[39–42] The crystal structure of β-Bi_2O_3 exhibits irregular bond lengths, leading to the formation of BiO_4 tetrahedra with non-uniform shapes and resulting in the creation of extensive straight tunnels throughout the lattice. Such intrinsic ionic conduction capability and moisture resistance make it a promising candidate for functionalizing biosensors with washability without sacrificing sensing performance.

Herein, we present a washable ion-selective biosensing device that uses nanostructured β-Bi_2O_3 with moisture resistance and fast ionic conductance. Following a systematic study on the oxide structural and phase engineering, we found that β-Bi_2O_3 nanoflakes added to the ion-selective layers via the electrochemical deposition method provide optimized washing stability without introducing large impedance. The controllable method also provides compatibility for preparing a variety of washable biosensors, such as sodium (Na^+), potassium (K^+), and pH sensors for sweat analysis (Table S1).[43–48] The as-fabricated Na^+ sensors deliver a sensitivity of 58.70 mV/dec with a performance retention of over 90% after 20 washing cycles. Moreover, a wireless epidermal sweat-sensing wristband that is washable and reusable was demonstrated by integrating the ion-selective sensors onto a textile platform. The as-developed strategy for washable biosensor fabrication and the in-depth study of the underlying mechanisms would open up opportunities for the advancement of practical e-textiles.

RESULTS AND DISCUSSION

Design and fabrication of textile-based washable ion-selective sensors

The textile-based washable biosensors are fabricated on a piece of commercial polyester (PET) cloth in a facile and scalable process. As illustrated in Figure 1A, the PET cloth was metalized into a conductive copper (Cu) cloth via rapid polymer-assisted metal deposition treatment and patterned into two electrodes via in-textile photolithography.[49–52] The biosensors in such a two-electrode configuration comprise an ion-selective electrode (ISE) and an Ag/AgCl solid reference electrode. The ISEs generate the corresponding potential difference to the reference electrode in different ion concentrations due to the varying ionic strengths. Afterward, by optimizing the electrolyte formulation and applied voltage parameters, β-Bi_2O_3 nanoflakes are added to the ion-selective membrane (ISM). Figures 1B and 1C show a photograph of the as-fabricated textile-based washable ion-selective sensors.

The optimization of the structures and active material mass loading of each functional layer in the working electrodes plays a critical role in the sensitivity and washability of the sensors. As displayed in Figure 1D, the Cu electrode patterns on textiles were texturized with nanodendritic gold (Au) with enhanced conductivity and large surface areas (morphology shown in Figures S1A–S1C).[53,54] Due to the special 3D architecture of textiles, which results in increased contact resistance and limited active potential, the yielding of biosensors with high sensitivity is relatively low. Compared to biosensors with thin-film layers, the Au nanostructured layers deliver an enhanced signal value with a sensitivity of 59 mV/dec and the lowest limit of detection of 0.3125 mM (Figures S2A, S2B, and S1D). Poly(3,4-ethylenedioxythiophene) polystyrene sulfonate (PEDOT:PSS) as the transducer layer was dip coated with optimized loading to ensure full coverage on the nanostrutured Au layers so as to avoid metal polarization that could result in signal drift. The resulting sensor has a drift of around 2.37 mV/h at a concentration of 40 mM (Figures S1E and S2C). The ISM on the top layer of the sensors (Figure S1F) is then uniformly incorporated with β-Bi_2O_3 nanoflakes, as shown in the scanning electron microscope (SEM) images of Figure 1E. The β-Bi_2O_3 nanoflakes distributed through the ISM also serve as the anchors to enhance the adhesion between the membrane and PEDOT:PSS layer. The robust interface minimizes the risk of membrane delamination under the mechanical interference during the washing process. Moreover, the β-Bi_2O_3 nanoflakes facilitate smooth ion contacts so that the ionophore N_c in the membrane can specifically absorb target ions M^+ to form ion group MN_c^+. The ion groups of MN_c^+ then migrate to the membrane/transducer interface and transfer electrons to the conductive layers, thus generating the potential difference to the reference electrode.[55] The X-ray diffraction (XRD) analysis and X-ray photoelectron spectroscopy (XPS) spectra confirm that β-Bi_2O_3 nanoflakes can be successfully deposited onto the Au electrodes on PET cloth (Figures 1F and S3).

To investigate the fast ion-conducting properties of the β-Bi_2O_3-nanoflake-functionalized ISM, their molecular structures were analyzed. As shown in the transmission electron microscopy (TEM) images (Figures 1G and S4), the lattice distance along the (201) crystal plane is 0.32 nm, which is consistent with XRD analysis and confirms the formation of β-Bi_2O_3 (PDF#78-1793) with a tunneling structure. Figure 1H shows the molecular structure of β-Bi_2O_3 with the distinctive tunneling structure that contributes to facilitating ion diffusion. In this molecular structure, the BiO_4 tetrahedra share corners to form large-size straight

Please cite this article in press as: Shi et al., Washable textile biosensors enabled by nanostructured oxides with fast ion diffusion, Device (2024), https://doi.org/10.1016/j.device.2024.100503

CellPress
OPEN ACCESS

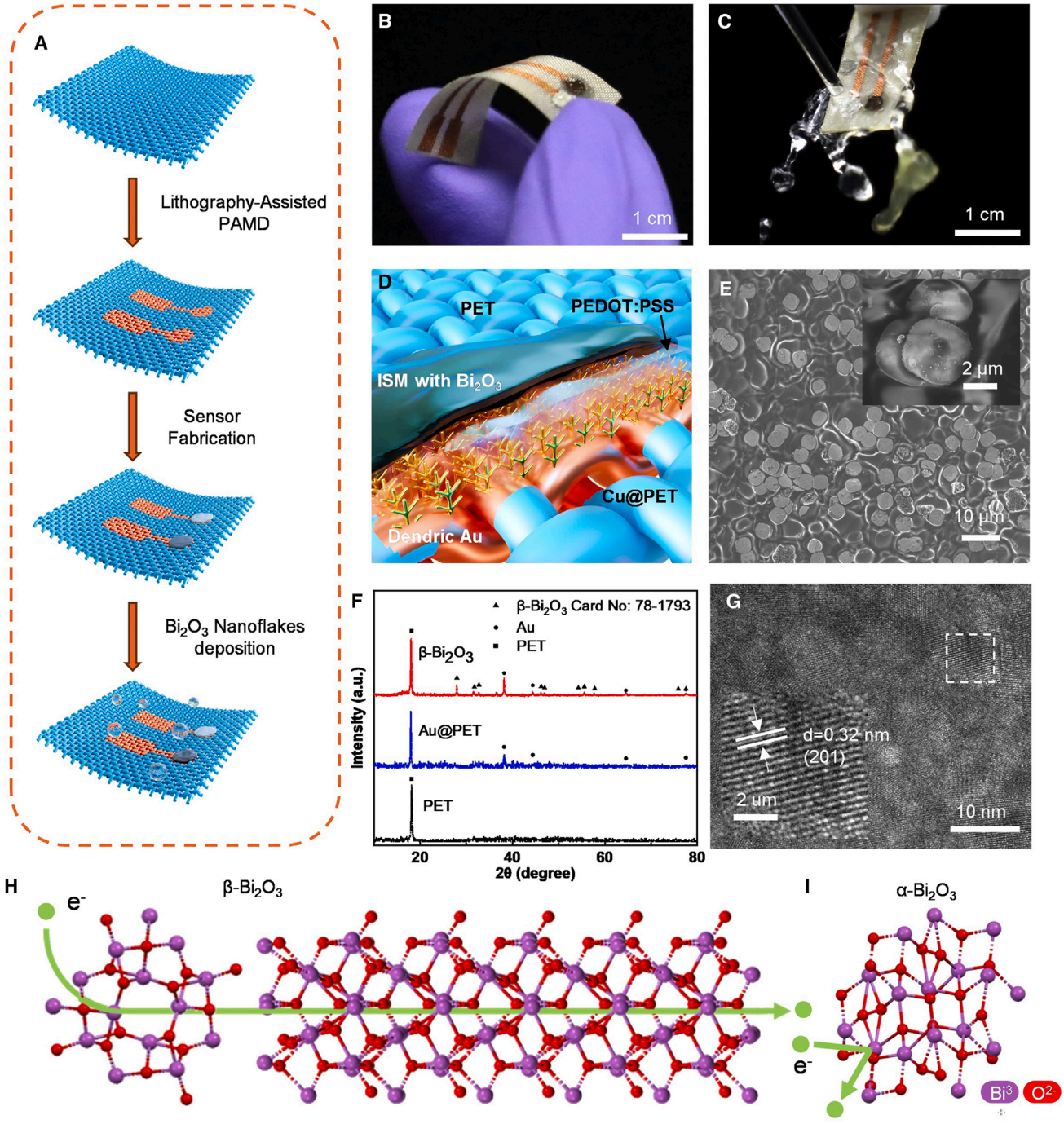

Figure 1. Fabrication process and mechanisms of the washable textile-based ion-selective biosensors

(A) The fabrication process of textile-based ion-selective sensors.

(B) Photo of the textile-based ion-selective sensor consisting of working and reference electrodes.

(C) Photo indicating the washability of the sensor.

(D) Schematic illustration of the sensing mechanism of β-Bi_2O_3-nanoflake-functionalized sensors.

(E) SEM images showing the morphology of β-Bi_2O_3 nanoflakes approximately 4.14 μm in diameter.

(F) XRD spectrum of the β-Bi_2O_3 deposited on Au@PET cloth.

(G) The high-resolution transmission electron microscopy images of β-Bi_2O_3.

(H and I) Molecular structures of (H) β-Bi_2O_3 and (I) α-Bi_2O_3.

Please cite this article in press as: Shi et al., Washable textile biosensors enabled by nanostructured oxides with fast ion diffusion, Device (2024), https://doi.org/10.1016/j.device.2024.100503

tunnels through the crystal, providing the shortest path for the ions to migrate across the ISM. In contrast, α-Bi_2O_3 with the monoclinic phase can be prepared with a lower electrochemical deposition potential of -0.4 V, which forms longer electron transport paths, as shown in Figure 1I.[56] It is also observed that with low deposition potential, the oxidation process is not completed, and meta-Bi was also deposited on the ISM (Figure S5). The α-Bi_2O_3 and meta-Bi composites could introduce relatively large impedance and polarization on the ISM and, thus, result in reduced levels of signals (Figure S6). Therefore, the moisture-resistive β-Bi_2O_3 nanoflakes with fast ion-conducting capability that was synthesized via rational structural and phase engineering can be applied for washable sensors.

Sensing performance optimization and characterization of the β-Bi_2O_3-functionalized ion-selective sensors

To validate the role of β-Bi_2O_3 nanoflakes, we fabricated and measured different sensors functionalized with a series of metal oxides in different morphologies and device architectures, as illustrated in Figure 2A. To evaluate the contribution of the moisture-resistance and ion-conducting properties of the oxides, MnO_2 nanoflakes with high hydrophobicity and MgO with corrosion resistance were electrochemically deposited onto the ISM for comparison with β-Bi_2O_3 nanoflakes.[57–60] The sensor coated with MnO_2 exhibited a higher contact angle (CA) of around 105° compared to the bare sensor, which had a CA of about 87°, indicating enhanced hydrophobicity (Figure S7). The open circuit potential (OCP) was measured for sensors exposed to NaCl solutions at varying pH values to assess the corrosion resistance conferred by MgO coating[61] (Figure S8). The OCP data revealed that the bare silver electrodes showed a gradual decrease in potential. In comparison, the MgO-coated electrodes maintained more stable potentials except at more acidic pH values, particularly below pH 5, which likely leads to neutralization reactions between the oxides and acidic solutions. Besides, anti-corrosive Al_2O_3 films commonly used as protective layers were prepared via magnetron sputtering, compared with Bi_2O_3 thin films, to study the influences of morphology and regional distribution on different active layers. The morphologies of ISM functionalized with different nanostructured oxides and planar thin films are shown in Figures 2B and S9.

The sensing responses of the Na^+ ion-selective sensors were characterized in standard solutions with concentrations ranging from 160 to 10 mM, as shown in Figure 2C. Although the sensors with MnO_2 show slightly enhanced washing stability (Figure S10), its large impedance results in reduced levels of signals and sensitivities. For sensors with MgO, the responses do not follow a linear correlation with the ion concentration. Besides, the sensors with α-Bi_2O_3 thin films on the ISM and PEDOT:PSS layer show device failures, possibly due to the prohibited ion pathway with such bulky protective layers (Figure 2D). The XRD analysis of α-Bi_2O_3 thin films, depicted in Figure S11, was conducted using high-temperature-resistant commercial PET instead of the original textile to prevent substrate damage during the evaporation process. Non-ideal sensing responses were also observed on sensors with Al_2O_3 thin films. The results of the sensing performance of ion-selective sensors with different oxide morphologies and regional distribution were summarized in Figure S12. Moreover, the sensor incorporating β-Bi_2O_3 nanoflakes displayed higher adhesion strength at the ISM and electrode interface. As shown in Figure 2E, it requires the highest applied force to delaminate the ISM from the sensors. Thus, we conclude that the β-Bi_2O_3 nanoflakes serve as the fast ion conductor to maintain the high sensitivity of the sensors while enhancing the mechanical stability.

The Na^+ sensors with β-Bi_2O_3 nanoflakes exhibit a sensitivity of 59 mV/dec with desirable recoverability, which refers to testing from high to low concentrations (160, 80, 40, 20, and 10 mM) and then from low to high (10, 20, 40, 80, and 160 mM), where the output voltage for the same concentration remains consistent (Figure S2D). The sensors deliver increased amplitudes of output signals and reduced impedance compared to sensors without β-Bi_2O_3 nanoflakes (Figures 3A–3B), which can be attributed to the fast ion conductance property. The results indicate that the additional protective material of β-Bi_2O_3 nanoflakes does not compromise the original sensing performance. Figure 3C demonstrates good reproducibility of the Na^+ sensor fabricated using the proposed process, with a relative standard deviation (RSD) of 1.4% in the sensing range of 10–160 mM. The selectivity of the sensor is also investigated to ensure that the interference biomarkers (such as H^+, K^+, NH_4^+, and Cl^-) in sweat have a limited effect on biomarker monitoring (Figures 3D and S13A). Besides, the test solutions with varying pH values are used to simulate the pH range of human sweat, thus demonstrating the reliability and accuracy of the sensor in applications related to monitoring human health (Figure S13B). The sensors demonstrate robust stability across a range of environmental humidity conditions, maintaining consistent performance metrics without significant variation in output, thereby underscoring their suitability for deployment in diverse atmospheric settings (Figures S13C and S13D). The biosensors are utilized for continuous monitoring of artificial sweat with varying concentrations of Na^+ for up to 2.5 h, demonstrating stability in real-time and long-term human health monitoring applications (Figure S2E). Moreover, the as-fabricated textile sensors demonstrate a remarkable shelf life with negligible sensitivity changes over 20 days, with a minimal RSD of 0.08% (Figure 3E). The mechanical stability of the textile sensors was evaluated under bending cycles of 50, 100, 150, and 200, and negligible response variation was observed (Figure 3F). Such desirable performances ensure reliable applications for real-time epidermal sweat sensing.

The wearing comfort of the washable textile sensors was evaluated with large-scale sensing electrodes, as shown in Figures 3G and 3H. The water vapor permeability (WVP) was tested using the cup method based on the ASTM E96 (procedure B) testing standard (ASTME96-00, 2000). Four pieces of textiles, namely the original PET cloth, Cu-deposited PET (Cu@PET) cloth, Cu@PET cloth with ISM, and the one functionalized with β-Bi_2O_3 nanoflakes, were placed on top of a bottle of water in an airtight manner. Another bottle of water without any covering was used as a reference. The water evaporation through textiles was evaluated by comparing the initial weights of each bottle and the values after 20 days. It is observed that the presence of β-Bi_2O_3 nanoflakes has contributed to an additional 6.47% of trapped moisture compared with the cloth

Please cite this article in press as: Shi et al., Washable textile biosensors enabled by nanostructured oxides with fast ion diffusion, Device (2024), https://doi.org/10.1016/j.device.2024.100503

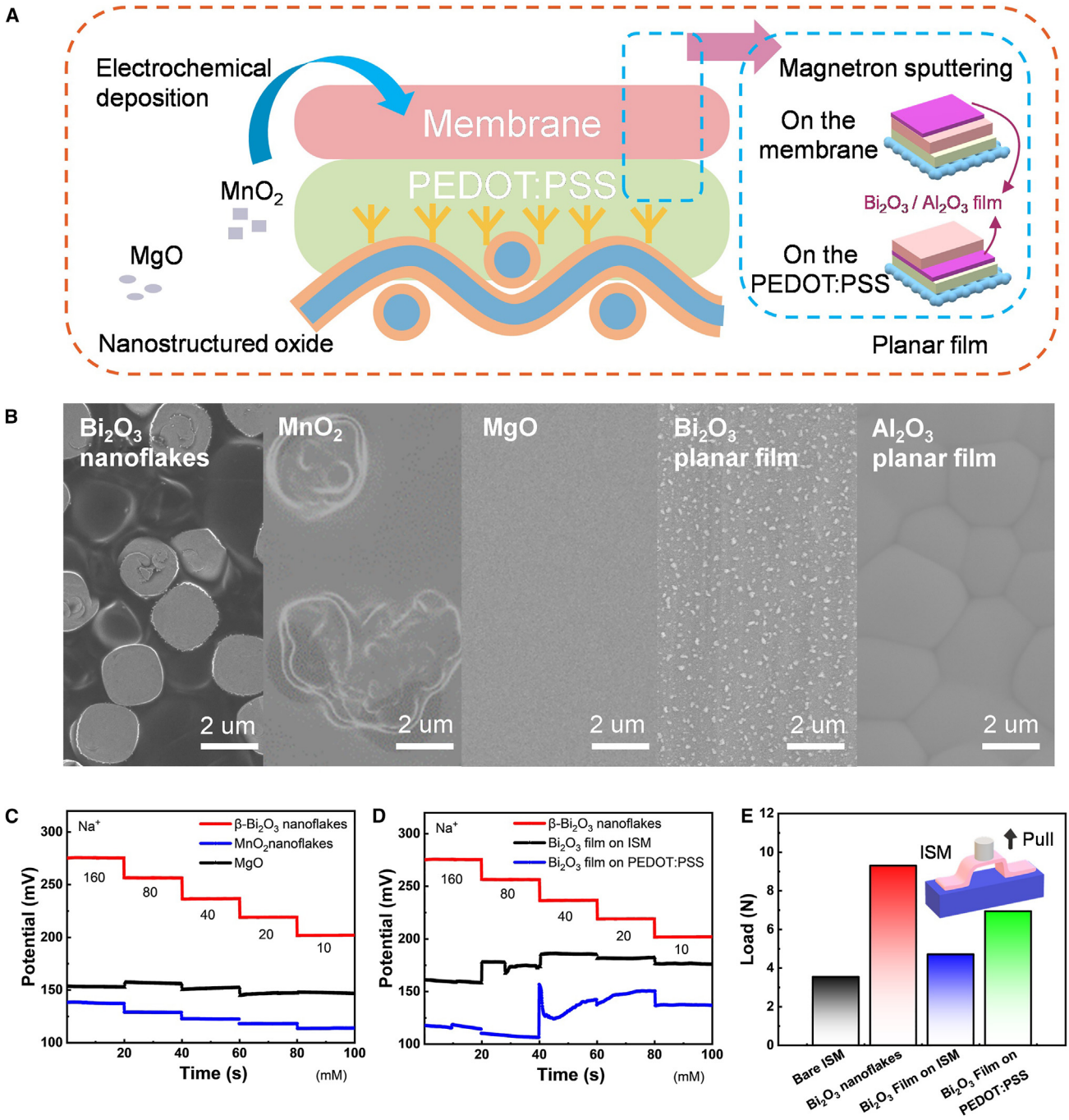

Figure 2. Optimization and schematic illustration of the protective layer of the ISM

(A) The schematic of the protective layer with a series of metal oxides in different morphologies and device architectures.

(B) SEM morphology of β-Bi_2O_3 nanoflakes, MnO_2 nanoflakes, MgO, α-Bi_2O_3 planer film, and Al_2O_3 planar film on the ISM.

(C and D) Performance evaluation of Na^+ ion-selective sensor with different metal oxides and Bi_2O_3 in different morphologies and positions.

(E) Adhesion strength of ISM with Bi_2O_3 in different morphologies and device architectures.

without the nanoflakes. The 3D porous structure of the textile maintains moisture breathability even with the integration of washable biosensors. The water vapor was observed to pass through the textile sensing patch cover on top of the boiling water (Figure 3I).

Evaluation of sensor washability

To investigate the effect of β-Bi_2O_3 nanoflakes on the washability of biosensors, we evaluated the sensing performance after different durations of washing. Figure 4A shows that contamination on the textile-based sensors can be cleaned up with a direct

Please cite this article in press as: Shi et al., Washable textile biosensors enabled by nanostructured oxides with fast ion diffusion, Device (2024), https://doi.org/10.1016/j.device.2024.100503

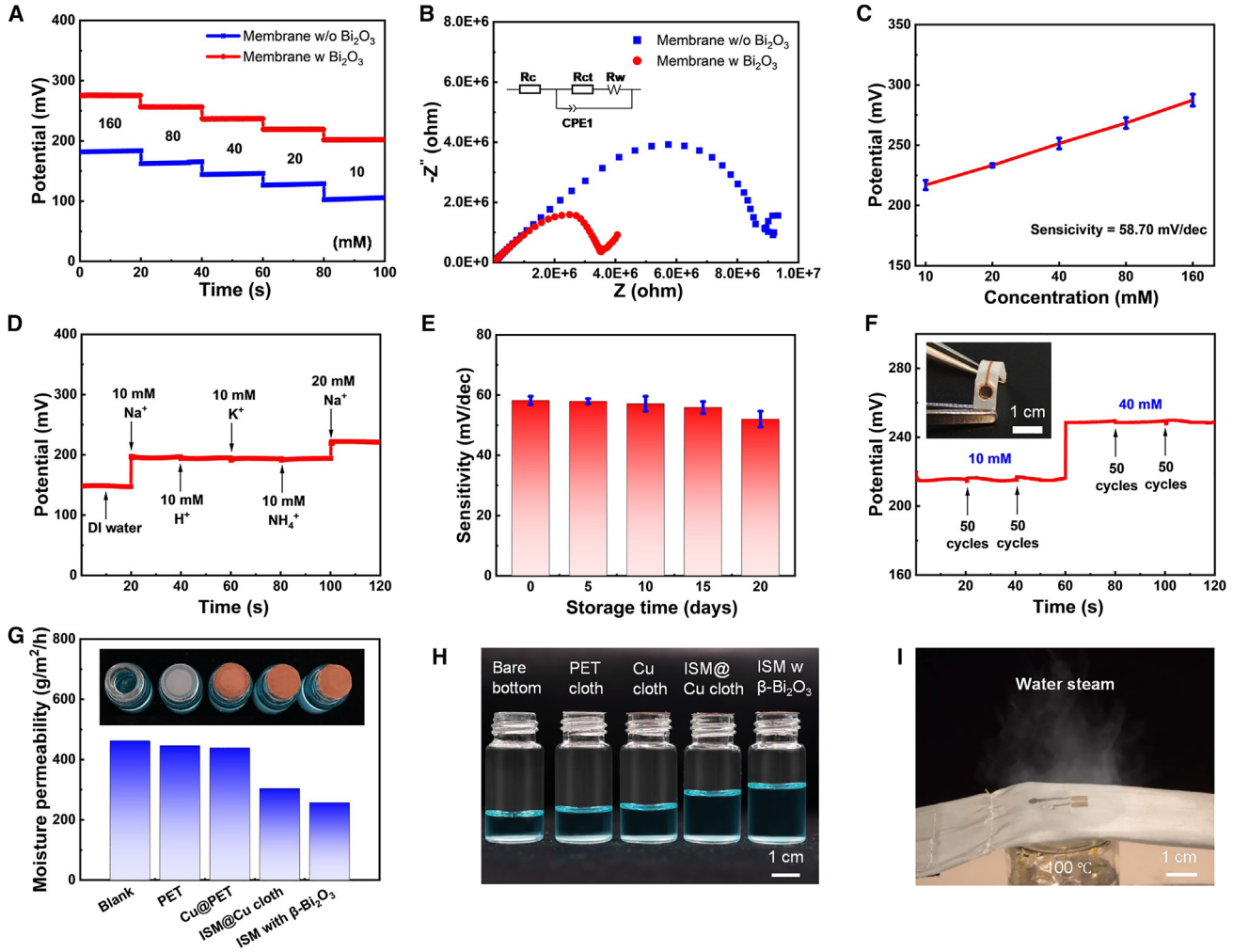

Figure 3. Performance evaluation of textile-based Na^+ ion-selective sensor

(A) Comparison of Na^+ sensor performance with and without β-Bi_2O_3 nanoflakes.

(B) Electrochemical impedance spectroscopy curves of the selective membrane with and without β-Bi_2O_3.

(C) Reproducibility of the sensors functionalized with β-Bi_2O_3 nanoflakes. The error bars represent the RSD of the evaluated sensitivity from five samples.

(D) Selectivity.

(E) Long-term storage stability. The error bars represent the RSD of the evaluated sensitivity from three samples.

(F) Bending stability.

(G) Moisture permeability tests.

(H) Photo corresponding to (G) indicating the remaining water quantity in the bottles covered with different samples.

(I) Water vapor test of a wristband integrated with the washable sensors.

water rinse. To achieve a more controllable washing stability test, a standard process simulating the machine washing was set up by merging the sensor in deionized (DI) water within a beaker and controlled by a magnetic rotor with a speed of 1,800 rpm for a duration of 30 s, as visualized in Figure 4B. The surface morphologies of the biosensors after 20 washing cycles were characterized by SEM. The ISM functionalized with β-Bi_2O_3 nanoflakes was preserved (Figure 4C). In contrast, the bare ISM showed delamination and exposed the underlying PEDOT:PSS layer (Figure 4D). This indicates that β-Bi_2O_3 nanoflakes can serve as the physical shield to preserve the sensors' structural integrity.

The sensing performances of the sensors with and without the incorporation of β-Bi_2O_3 were examined after every two washing processes, as shown in Figure 4E. The bare Na^+ sensor showed a large variation in response signals and decreased sensitivity after each washing cycle and completely deteriorated after six cycles. In comparison, the sensors with β-Bi_2O_3 nanoflakes deliver a sensitivity retention of >90% within 20 washing cycles (Figure 4F) and >70% retention after 50 cycles (Figure S14). The sensors show minimal signal drift down to 3.85 mV/h (Figure 4G) and baseline drift lower than 10% (Figure S15). In contrast, the sensors without β-Bi_2O_3 nanoflakes exhibited around 10 times larger signal drift and a baseline drift of up to 650%. The effectiveness

Please cite this article in press as: Shi et al., Washable textile biosensors enabled by nanostructured oxides with fast ion diffusion, Device (2024), https://doi.org/10.1016/j.device.2024.100503

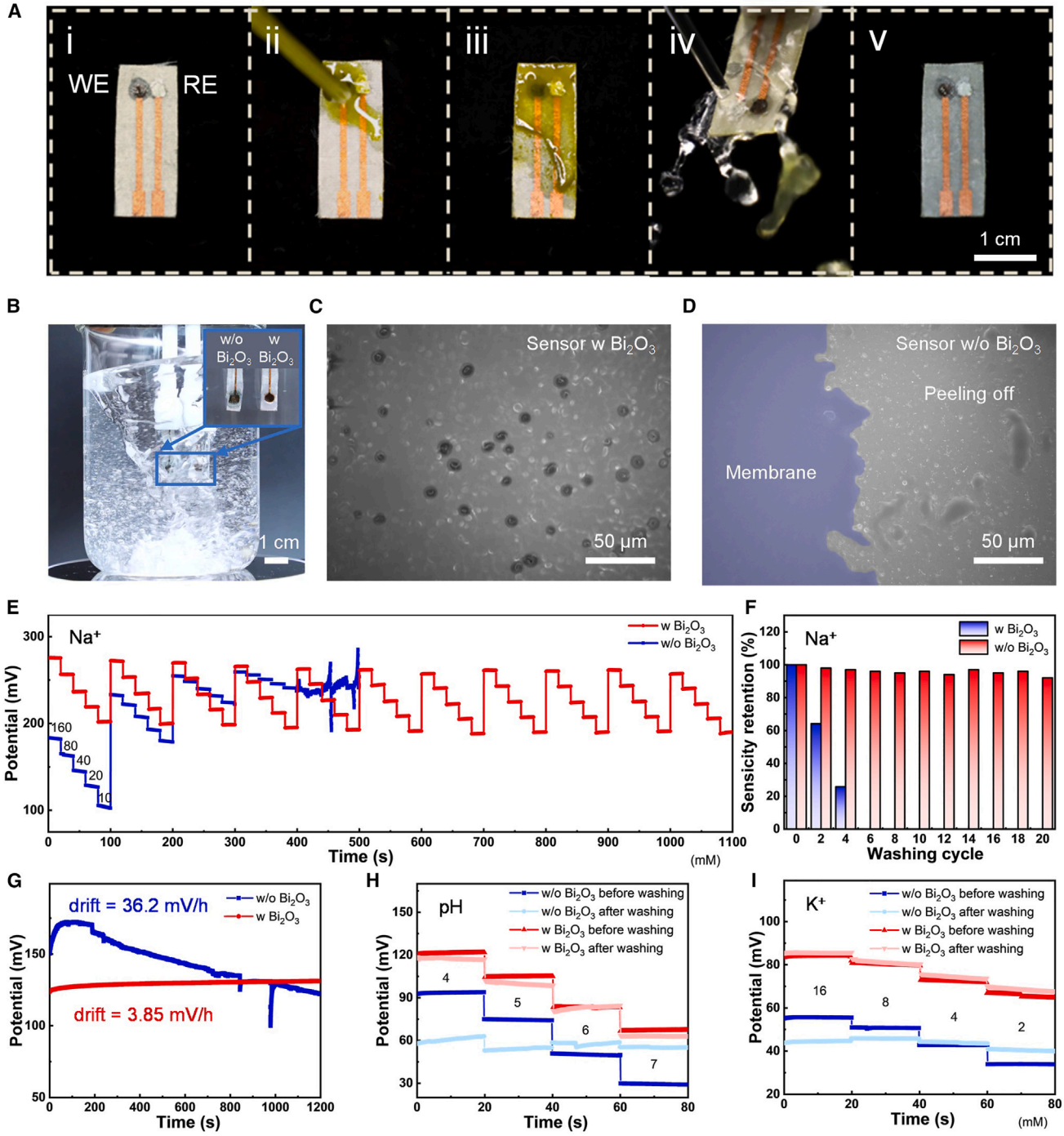

Figure 4. Washability enhancement by β-Bi_2O_3 nanoflakes

(A) Pictures showing the sensor being contaminated and washed: (i) sensor with a clean surface, (ii) applying stains to the sensor, (iii) sensor with stains on the surface, (vi) rinsing with water, and (v) cleaned sensor.

(B) Photo of the standard process simulating the machine-washing process.

(C and D) SEM photos of biosensors with and without β-Bi_2O_3 nanoflakes after washing for 300 s.

(E) The sensing responses of Na^+ sensor with and without β-Bi_2O_3 nanoflakes after washing process.

(F) Comparison of sensitivity retention during the washing process.

(G) Signal drifts of sensors with and without β-Bi_2O_3 after washing.

(H and I) Washability enhanced by β-Bi_2O_3 nanoflakes on K^+ and pH sensors (performance conducted before and after 5 washing cycles).

Please cite this article in press as: Shi et al., Washable textile biosensors enabled by nanostructured oxides with fast ion diffusion, Device (2024), https://doi.org/10.1016/j.device.2024.100503

of β-Bi_2O_3 nanoflakes for preparing washable biosensors is also demonstrated on the highly selective K^+ and pH sensors, which were subjected to five washing cycles. The outcomes, detailed in Figures 4H–4I, demonstrate the robustness and compatibility of the proposed method, ensuring sustained sensor functionality after washing.

Additionally, experiments were conducted to evaluate sensor performance in different detergents, such as laundry detergent and soapy water. The results show that biosensors functionalized with β-Bi_2O_3 nanoflakes can help maintain functionality and enhance washability and durability across these diverse washing conditions (Figure S16). A standard washing process was performed according to AATCC Standard LP1-2021 on a textile integrated with a bare biosensor and another one functionalized with β-Bi_2O_3 nanoflakes (Figure S17A). The sensors were washed at 40°C for 21 min with a fabric load of 1.6 kg using a top-loading washing machine (CHIGO, XQB65-3801), as demonstrated in Video S1. It is observed that the bare ISM was peeled off after washing, while the ISM functionalized with β-Bi_2O_3 nanoflakes remained intact (Figures S17B–S17D). This contributes to a sensitivity retention of above 80% of the washable sensors (Figures S17E and S17F).

Based on the above systematic characterization of the textile-based ion-selective sensors, the underlying mechanisms for enhanced washability with β-nanoflakes were proposed. Bi_2O_3 provides chemical stability and hydrophobicity to facilitate water repellency and prevent water-induced degradation. However, its relatively large impedance would sacrifice the sensing sensitivity. To reduce the impedance and ensure smooth ion diffusion through the sensor active layers, engineering the oxides into β-Bi_2O_3 gives rise to the fast ion conductance property. Besides, the nanoflake structures further reduced the impedance while anchoring the selective membrane. As indicated by the CA measurements, the incorporation of β-Bi_2O_3 nanoflakes onto the ISM contributes to a more stable hydrophobic properties. As depicted in Figure S18, for sensors functionalized with β-Bi_2O_3 nanoflakes, the CA was maintained at around 105° before washing and slightly decreased to about 93° after five wash cycles. In contrast, sensors without β-Bi_2O_3 exhibited a significant decline in hydrophobicity, with the CA dropping from 87° to 57° after the same washing process.

Application demonstration

Integrated textile sensing wristband for wireless epidermal sweat sensing

To achieve real-time and wireless sweat analysis, a washable textile-based wristband is designed and fabricated. The wristband consists of an in-textile washable biosensor for highly selective Na^+ monitoring, a pocket for integration with a removable flexible circuit, and a battery (shown in Figures 5A and S19). To extract the OCP biosignals, a high-impendence potential detection circuit was designed to realize signal processing with suppressed interferences, combined with a Bluetooth module for wireless transmission. Figure S20 illustrates the assembly of the integrated wristband. Because of its breathability and flexibility, our textile biosensing wristband is more comfortable to wear compared to a smartwatch with rigid electronics or a flexible device that adheres directly onto the skin. As shown in Figure 5B, after wearing the wristband on the forearm for 4 h, no visible allergic contact dermatitis was observed under the textile wristband region. In contrast, it was observed that the smartwatch resulted in moisture accumulation and skin irritation, while the flexible circuit with medical adhesive tape caused pronounced skin erythema, possibly due to its poor air permeability and high adhesion strength. The wristband can be washed after the removal of the circuit and battery module, as shown in Figures 5C and 5D, and the sensing performance of the wristband was maintained after washing (see Video S2).

The washable textile wristband was tested for sweat Na^+ monitoring during physical exercise with a wireless mobile app for remote tracking (Figures 6A and 6B). The flow of the systematic circuit design is outlined in Figure 6C. Following the acquisition of the output analog signals from the electrochemical sensor, a voltage follower was utilized to eliminate signal interference. By employing impedance matching for signal amplification and filtering modules, precise resolution of the output signal within the range of the analog-to-digital converter was achieved. A microcontroller with computational and serial communication capabilities was used to calibrate, compensate, and transmit the extracted signals to an onboard wireless transceiver. The transceiver facilitated wireless data transmission to a Bluetooth-enabled mobile handset equipped with a custom-developed app. Real-time graphical representations of received data strings and automatic data downloads were performed by the mobile app to enhance user friendliness. The extraction of Na^+ sensor signals commenced after a warm-up period of 20 min. Real-time tracking of sweat Na^+ variation is visually represented in Figure 6D. Tests involving different exercise intensities for the same subject were performed, as shown in Figure 6E. The extracted sweat Na^+ concentrations were validated using inductively coupled plasma mass spectrometry (ICP-MS), which showed a similar tendency. The demonstration for sweat ion analysis indicates the promising application of the as-fabricated washable biosensing wristband for reusable, non-invasive health monitoring.

Conclusions

Textile-based integration electronics need to maintain functionality after cycles of washing. When measuring epidermal biomarkers, the sensors are highly sensitive to mechanical interferences and cannot be reliable if the active materials are lost during washing. In this work, we designed a biosensor using ion-selective sensing electrodes that are electrochemically functionalized with phase-engineered β-Bi_2O_3 with biocompatibility.[31–35] Previous studies have shown that β-Bi2O3, commonly used as a dental filling material, is non-toxic and safe for the human body. The β-Bi_2O_3 nanoflakes added to the ion-selective layers serve as the protective layer and also provide straight tunneling pathways for fast charge transport without blocking the ion contacts, with enhanced washability and sensitivity. We demonstrated washable textile-based ion-selective biosensors and integrated these sensors

Please cite this article in press as: Shi et al., Washable textile biosensors enabled by nanostructured oxides with fast ion diffusion, Device (2024), https://doi.org/10.1016/j.device.2024.100503

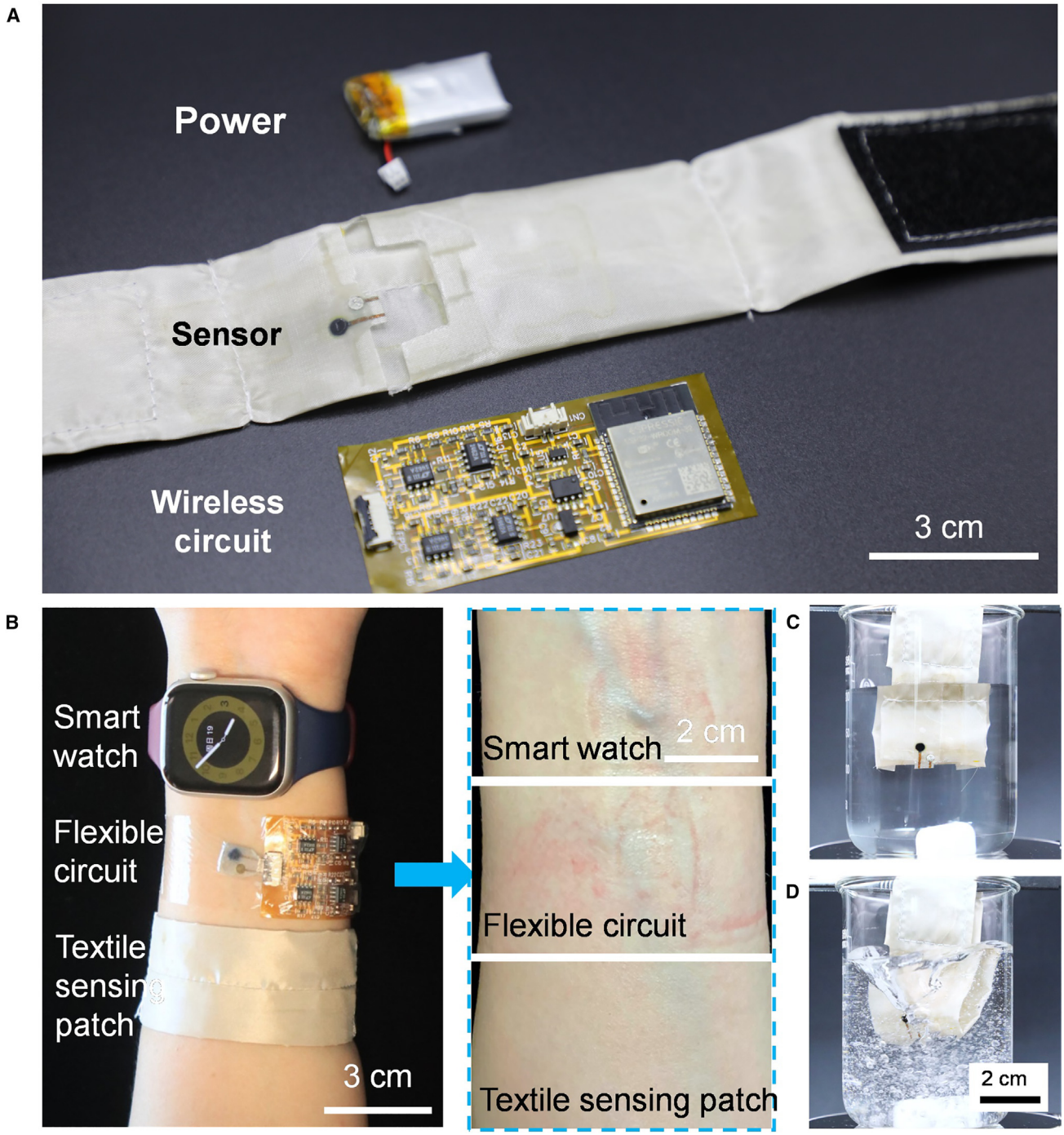

Figure 5. Demonstration of the washable textile wristband for sweat monitoring

(A) Photograph showing the components of the sensing wristband, including the in-textile ion-selective sensor, removal circuit, and battery modules.
(B) Photographs showing the skin irritation tests by wearing a smartwatch, a flexible circuit, and the as-fabricated textile wristband on the forearm.
(C and D) Photographs showing the washing process of the wristband.

into washable and wearable e-textiles that provide comfort, real-time sensing, and wireless communication. This facile electrochemical approach for functionalizing biosensors with washability should be compatible for a variety of ion-selective biosensors. The proposed strategy to realize washable textile-based biosensors would also inspire future research efforts to realize multi-functional modules with enhanced washability.

Please cite this article in press as: Shi et al., Washable textile biosensors enabled by nanostructured oxides with fast ion diffusion, Device (2024), https://doi.org/10.1016/j.device.2024.100503

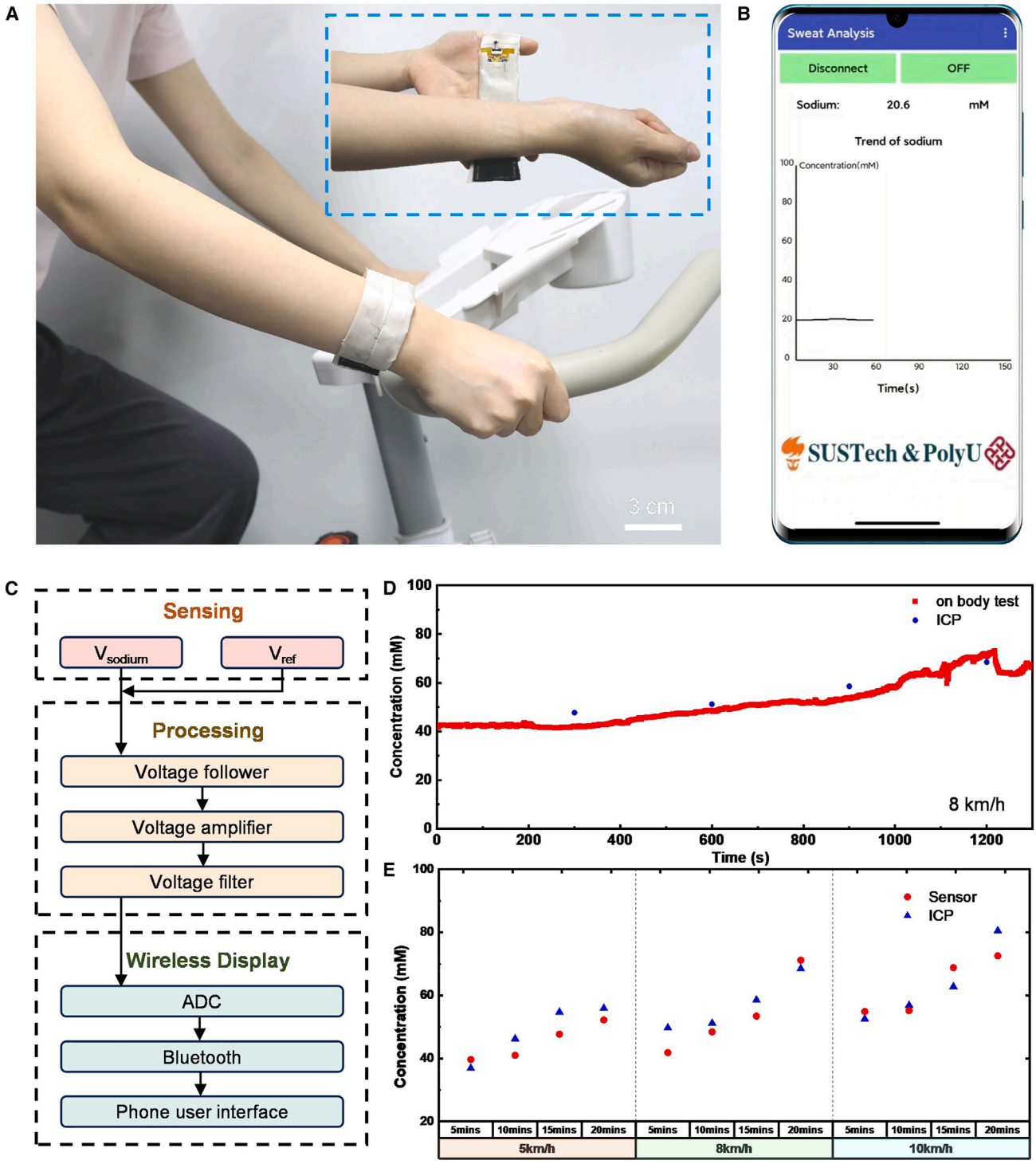

Figure 6. On-body demonstration of the washable textile wristband for sweat monitoring

(A) Photograph showing *in situ* sweat monitoring with the integrated textile wristband during exercise.

(B) Custom-designed mobile application for real-time and remote tracking.

(C) The logical flow of the systematic design for real-time and wireless Na^+ sensing.

(D) The real-time monitoring of sweat Na^+ concentrations during 8 km/h cycling exercise obtained with the wristband and results validated with ICP.

(E) Comparison of sweat Na^+ sensing results with the wristband and validated ICP values at different cycling speeds of 5, 8, and 10 km/h every 5 min.

Please cite this article in press as: Shi et al., Washable textile biosensors enabled by nanostructured oxides with fast ion diffusion, Device (2024), https://doi.org/10.1016/j.device.2024.100503

EXPERIMENTAL PROCEDURES

Resource availability

Lead contact

Further information and requests for resources, data, and materials should be directed to and will be fulfilled by the lead contact, Yuanjing Lin (linyj2020@sustech.edu.cn).

Materials availability

All materials generated and used in this study are available upon sensible request to the lead contact.

Data and code availability

All data and code generated and used in this study are available upon sensible request to the lead contact.

Materials

Sodium hydroxide (NaOH), ethyl alcohol, acetic acid, 3-(trimethoxysilyl) propyl methacrylate (KH570), copper sulfate pentahydrate ($CuSO_4 \cdot 5H_2O$), bismuth standard solution (for AAS, 1,000 $\mu g\ mL^{-1}$ in 1.5 M HNO_3), manganese acetate ($MnAC_2$), ammonium acetate (NH_4Ac), dimethyl sulfoxide (DMSO), methacrylatoethyl trimethyl ammonium chloride (METAC), acetate buffer solution (ABS), potassium peroxodisulfate ($K_2S_2O_8$), ammonium tetrachloropalladate(II), 2,2-bimethoxy-2-phenylacetophenone (DMPA), N,N′-methylenebisacrylamide (NMBA), potassium sodium tartrate, copper sulfate pentahydrate, formaldehyde solution, and chloroauric acid ($HAuCl_4$) were purchased from Sigma-Aldrich. Hydrochloric acid (HCl), bis(2-ethylehexyl) sebacate (DOS), sodium tetrakis[3,5-bis(trifluoromethyl)phenyl]borate (Na-TFPB), high-molecular-weight polyvinyl chloride (PVC), magnesium sulfate ($MgSO_4$) valinomycin (potassium ionophore), $(NH_4)_2PdCl_4$, cyclohexanone, and tetrahydrofuran were purchased from J&K Scientific. PEDOT:PSS (PH1000), potassium ferricyanide(III), chloroauric acid, silver paste, polyvinyl butyral resin BUTVAR B-98 (PVB), sodium chloride (NaCl), iron(III) chloride ($FeCl_3$), and potassium chloride (KCl) were purchased from Aladdin Biochemical Technology. All other chemicals were commercially available and used without further purification. All solutions were prepared using DI water (16 M Ω cm) produced from a Millipore water purification system.

Fabrication of Cu-PET cloth

The textiles underwent a cleaning process using ultrasonication baths with acetone, isopropanol, and water for 15 min each time. Subsequently, the textiles were immersed in an ethanol solution consisting of 2.0 g L^{-1} DMPA, 16.0 g L^{-1} NMBA, and 30.0 mL L^{-1} METAC for a period of 1 min. Following this step, the textiles were exposed to ultraviolet (UV) light from a lamp with an intensity of UVA 80.0 mW cm^{-2} for 1 min before being rinsed with water for another minute. Then, the modified textiles were dipped in a solution containing 3.2 g L^{-1} $(NH_4)_2PdCl_4$ for 1 min and rinsed again with water for another minute. The electroless plating bath used to coat the textiles with copper consisted of a mixture comprising equal parts of solution A and solution B. Solution A was composed of $CuSO_4 \cdot 5H_2O$ at a concentration of 52 g L^{-1} along with NaOH at a concentration of 48 g L^{-1} and $KNaC_4H_4O_6 \cdot 4H_20$ at a concentration of 117 g L^{-1}. Solution B was prepared by diluting formaldehyde (37%) in water, resulting in its concentration being measured as 9.5 mL L^{-1}. Finally, the catalyst-treated textiles were immersed in this plating bath for 120 min to achieve copper-coated textiles.

Metallic electrode patterning

To begin, a layer of photoresist (NR9-1500p, Futurrex, USA) was evenly applied onto the metallic textile using a dipping method. The textile was then subjected to heat in an oven at 120°C for 5 min to solidify the photoresist. Next, the textile sample underwent exposure to double-sided UV light for 1 min using identical masks and received another round of heating in an oven at 120°C for 3 min to facilitate the reaction of the photoresist. Subsequently, the non-patterned area of the sample had its photoresist removed by employing a developer solution (RD6, Futurrex, USA). Following this step, etching of the metal in the non-patterned region took place utilizing a solution containing $FeCl_3$ with a concentration of 1 M. Finally, any remaining photoresist on top of the metal pattern was eliminated using acetone. To prepare these textiles with metallic patterns for subsequent processing steps, they were rinsed with alcohol and DI water before being air dried under normal conditions.

Fabrication of textile-based Na^+ sensors

First, the nanodendritic Au was fabricated on the metallic Cu electrodes using an electrolyte mixture comprising 50 mM $HAuCl_4$ and 50 mM HCl. The deposition was achieved by applying a periodic voltage wave with an amplitude of −2 V, a frequency of 50 Hz, and a duty cycle of 50% in the electrolyte for 9,000 cycles. To serve as the ion-electron transducer, PEDOT:PSS was deposited onto the working electrode. This deposition was achieved by drop casting 3 μL PEDOT:PSS (PH1000) onto the electrode. The Na^+ selective membrane cocktail consisted of Na ionophore X (1% w/w), Na-TFPB (0.55% w/w), PVC (33% w/w), and DOS (65.45% w/w). 100 mg of the cocktail was dissolved in 660 μL of tetrahydrofuran to prepare the membrane solution. ISMs were then prepared by drop casting 6 μL of the Na^+ selective membrane cocktail onto the PEDOT:PSS/Au electrode. For the reference electrode of the Na+ sensor, the Ag/AgCl electrode was modified by casting 10 μL of the reference solution onto it. The PVB reference electrode solution was prepared by dissolving 79.1 mg PVB and 50 mg NaCl in 1 mL methanol. The modified electrode was left to dry overnight.

Fabrication of textile-based K^+ sensors

First, the nanodendritic Au was fabricated on the metallic Cu electrodes using an electrolyte mixture comprising 50 mM $HAuCl_4$ and 50 mM HCl. The deposition was achieved by applying a periodic voltage wave with an amplitude of −2 V, a frequency of 50 Hz, and a duty cycle of 50% in the electrolyte for 9,000 cycles. To serve as the ion-electron transducer, PEDOT:PSS was deposited onto the working electrode. This deposition was achieved by drop casting 3 μL of PEDOT:PSS (PH1000) onto the electrode. The K^+ selective membrane cocktail consisted of valinomycin (2% w/w), Na-TPB (0.5% w/w), PVC (32.7% w/w), and DOS (64.7% w/w). 100 mg of the cocktail was dissolved in 350 μL of tetrahydrofuran to prepare the membrane solution. ISMs were then prepared by drop casting 6 μL of the K^+ selective membrane cocktail onto the PEDOT:PSS/Au electrode. For the reference electrode of the K^+ sensor, the Ag/AgCl electrode was modified by casting 10 μL of the reference solution onto it. The PVB reference electrode solution was prepared by dissolving 79.1 mg PVB and 50 mg NaCl in 1 mL methanol. The modified electrode was left to dry overnight.

Fabrication of textile-based pH sensors

The electrolyte mixture comprised 50 mM $HAuCl_4$ and 50 mM HCl for the growth of Au dendritic nanostructures. The deposition was achieved by applying a periodic voltage wave with an amplitude of −2 V, a frequency of 50 Hz, and a duty cycle of 50% in the electrolyte for 9,000 cycles. Polyaniline (PANI) deposition was realized under a periodic voltage wave with an amplitude of 0.9 V, a frequency of 1 Hz, and a duty cycle of 10% for 1,200 cycles in a fresh electrolyte containing 0.1 M distilled aniline in 1 M HCl. For the reference electrode, the Ag/AgCl electrode was modified by casting 10 μL of the reference solution onto it. The PVB reference electrode solution was prepared by dissolving 79.1 mg PVB and 50 mg NaCl in 1 mL methanol. The modified electrode was left to dry overnight.

Functionalization of β-Bi_2O_3 nanoflakes on the sensors

The bismuth plating solution consists of 0.1 M ABS with 50 mM NaCl (10 mL) and 10 mL bismuth standard solution (for AAS, 1,000 $\mu g\ mL^{-1}$ in 1.5 M HNO_3). It should be noted that before plating, the bismuth standard solution was added to the buffer solution under stirring. All solutions can only be used once and must be ready to use. The morphologies of bismuth oxide obtained with different solution ratios and deposition time are shown in the Figures S21 and S22. The electroplating process was conducted under −0.8 V for 240 s, which represents the optimal plating time determined by comparing the performance of sensors obtained through various plating durations (Figure S23). The cyclic voltammetry (CV) curve is shown in Figure S24A. To stabilize the ion-selective sensor, it was immersed in a solution containing 40 mM NaCl for 4 h before measurements. This conditioning process enhanced stability and minimized potential drift, ensuring optimal long-term continuous measurements.

Please cite this article in press as: Shi et al., Washable textile biosensors enabled by nanostructured oxides with fast ion diffusion, Device (2024), https://doi.org/10.1016/j.device.2024.100503

Table 1. Comparison table of the relative humidity of the saturated salt solution and its surrounding atmosphere

Relative humidity (%)	Saturated solution solute
23	CH_3COOK
33	$MgCl_2$
43	K_2CO_3
57	NaBr

The electroplating method for magnesium oxide and manganese oxide is the same, but the voltage is different.

Evaporation of α-Bi_2O_3 planar film

The α-Bi_2O_3 planar film was fabricated in an argon-oxygen mixed atmosphere using direct current magnetron sputtering technology (JDP350) at room temperature. The high-purity raw material of bismuth (99.9%) was used. The base pressure in the deposition chamber was evacuated to 10^{-3} Pa, and argon and oxygen gases were mixed with a total flow rate of 6.1 sccm (O_2:Ar = 20:1) to provide a deposition pressure of 0.5 Pa. The deposition power was controlled at 20 W; the thickness of the coating was approximately 1,000 Å with a deposition time of 527 s and a deposition rate of 1.9 Å/s.

Evaporation of Al_2O_3 planar film

The Al_2O_3 planar film was fabricated in an argon atmosphere using radio frequency magnetron sputtering technology (JDP350) at room temperature. The high-purity raw material of alumina (99.9%) was used. The base pressure in the deposition chamber was evacuated to 10^{-3} Pa, and the flow rate of argon was 6.1 sccm to provide a deposition pressure of 0.5 Pa. The deposition power was controlled at 80 W with a frequency of 5.26 MHz; the thickness of the coating was approximately 1,000 Å with a deposition time of 10,000 s and a deposition rate of 0.1 Å/s.

Functionalization of MnO_2 nanoflakes on the sensor

The electrolyte for the deposition was prepared by dissolving 0.01 M $MnAC_2$ and 0.02 M NH_4Ac in a solvent mixture of 90% DI water and 10% DMSO. MnO_2 was fabricated using an anodic electrodeposition method at a constant current of 0.5 mA cm^{-2} for 10 min.

Functionalization of MgO on the sensor

The MgO plating solution consisted of 0.1 M $MgSO_4$.The electroplating process was conducted under −1.5 V for 300 s. The CV curve is shown in Figure S24B.

Characterization

The morphologies of samples were observed by SEM (Hitachi TM3000 and Gemini 300), polarizing microscope (Nikon), and TEM (Talos F200X G2). The structures were observed by XRD (Rigaku Smartlab) and XPS (PHI 5000 Versaprobe III). Electrodeposition and sensor performance were performed by two types of electrochemical workstations (CHI 760e and Ivium Soft 4). In addition, the concentrations of the biomarker in the collected sweat samples were also validated using ICP-MS (Thermo Q Exactive). Moisture permeability tests for the samples were performed using the cup method according to the textile standard E96/E96M-13. The moisture transmission rate (g m^{-2} day) was determined by measuring the weight loss of the water vapor in a cup with its opening firmly covered by the tested specimen (testing duration of 20 days). Both air resistance and moisture permeability tests were performed at around 22°C and 63% relative humidity. The mechanical properties of the sensor and Cu-patterned cloth were tested using an Instron 5599 universal testing system. The electrical properties of the samples under different stretching states were investigated by a Keithley 2400 Sourcemeter coupled with a computer-controlled stretching motor. The washing process of the sensor was carried out by magnetic stirring equipment. The beaker contained an appropriate volume of DI water and was placed on the magnetic stirrer with a suitable-sized tile at the bottom. The sensor was securely positioned so that one end remained submerged in the water. The rotational speed of the magnetic stirrer was controlled at 1,500 rpm, and each washing cycle lasted for 30 s.

Calculation on the baseline drift

Baseline drift refers to a metric test deviating from its initial reference point over time. To quantify this factor, the following equation is employed:

$$\frac{\Delta V}{S} = \frac{V_{after\ washing} - V_{before\ washing}}{S}\ topology, \quad \text{(Equation 1)}$$

where S is the initial sensitivity of the sensor. In light of this equation, the extent of baseline drift could be accurately calculated within the context of this study.

Textile WVP test

The WVP was tested by the cup method based on the ASTM E96 (procedure B) testing standard (ASTME96-00, 2000). Textile samples were enclosed in a cup comprising water covered at the top by a cover ring to determine the weight loss by evaporation time (20 days). Textiles with different structures were placed in an airtight manner over the top of a cup. Another cup served as a reference. The weight of the cups was measured firstly at the start of the test and then periodically after 20 days by the balance with a resolution of 0.01 g to determine how much water was lost from the textile sample. WVP can be calculated using Equation 2:

$$WVP = \frac{(24 \times M)}{A \times T}\frac{g}{m^2 h}, \quad \text{(Equation 2)}$$

where M denotes loss of mass (g), T denotes the time interval (h), and A denotes cup internal area (m^2). The internal cup area was calculated using Equation 3 below, where d represents the cup's internal diameter (mm).

$$A = \frac{(\pi d^2)10^{-6}}{4} \quad \text{(Equation 3)}$$

Standard washing process

The standard washing process was carried out using a household washing machine (CHIGO, XQB65-3801) according to AATCC Standard LP1-2021, Home Laundering. The biosensors were put into a water-permeable protective sack. Each washing process was conducted with a fabric load of 1.6 kg using 20 mL of commercial liquid detergent (Bluemoon) at a quick-washing mode at 40°C with a duration of approximately 21 min, which included soaking, rinsing, and spin drying.

Humidity test

The performance testing of the biosensor under humidity change was conducted at a controlled temperature of 20°C, with the standard humidity levels provided by the atmosphere above saturated salt solutions (refer to Table 1). The biosensors were placed above the liquid surface of saturated salt solution. The current and potential variations of the sensor were then measured as the environmental humidity changed using CHI 760e.

On-body sweat monitoring

All experiments were performed according to the university guidelines (The Ethics Guidelines for Research Involving Human Subjects or Human Tissue from Southern University of Science and Technology, SUSTech Institutional Review Board, 2024PES106). On-body evaluation of analysis in sweat was performed on healthy volunteers aged between 24 and 26 years. For real-time sweat monitoring, the wristband was connected to the smartphone app via Bluetooth. Volunteers were first asked to wear the wristband and cycled for around 20 min as a warm-up process. After that, the volunteers performed a 20 min stationary cycling session. Meanwhile, the app connection was started to begin data recording, and decoded sweat analysis results were displayed on the cellphone. Sweat was simultaneously collected every 5 min for off-body ICP-MS validation.

SUPPLEMENTAL INFORMATION

Supplemental information can be found online at https://doi.org/10.1016/j.device.2024.100503.

ACKNOWLEDGMENTS

The authors acknowledge the financial support from the National Natural Science Foundation of China (62201243 and 52203318), the Shenzhen Science and Technology Program (grant no. RCYX20231211090432060), the Fundamental and Applied Research Grant of Guangdong Province (2021A1515110627), and the Shenzhen Stable Support Plan Program for Higher Education Institutions Research Program (20220815153728002). This work was also supported by the State Key Laboratory of Ultra-precision Machining Technology (1-BBXR), the RGC Senior Research Fellow Scheme of Hong Kong (SRFS2122-5S04), and the Hong Kong Polytechnic University (1-CD44 and 1-ZVQM). We would like to acknowledge the technical support from SUSTech CRF and thank Dr. Lin and Dr. Ho for their help with ICP and SEM analyses.

AUTHOR CONTRIBUTIONS

Y.L. and Z.Z. conceived the study. Y.S. designed and fabricated the whole system. K.Z. assisted with sensor fabrication. X.M. aided in the on-body demonstration. L.H. contributed to circuit system logic design. X.H. conducted the XRD test. P.W. and Y.Z. helped with the fabrication of metallic textiles. F.C. assisted in the permeability test. M.H. was responsible for photography. Y.L. and Z.Z. revised the manuscript, and all authors contributed to it.

DECLARATION OF INTERESTS

The authors declare no competing interests.

Received: April 18, 2024
Revised: May 3, 2024
Accepted: July 15, 2024
Published: August 9, 2024

REFERENCES

1. Xu, K., Lu, Y., and Takei, K. (2021). Flexible Hybrid Sensor Systems with Feedback Functions. Adv. Funct. Mater. *31*, 2007436. https://doi.org/10.1002/adfm.202007436.
2. Krawczyk, K., Xue, S., Buchmann, P., Charpin-El-Hamri, G., Saxena, P., Hussherr, M.-D., Shao, J., Ye, H., Xie, M., and Fussenegger, M. (2020). Electrogenetic cellular insulin release for real-time glycemic control in type 1 diabetic mice. Science *368*, 993–1001. https://doi.org/10.1126/science.aau7187.
3. Yang, G., Deng, J., Pang, G., Zhang, H., Li, J., Deng, B., Pang, Z., Xu, J., Jiang, M., Liljeberg, P., et al. (2018). An IoT-Enabled Stroke Rehabilitation System Based on Smart Wearable Armband and Machine Learning. IEEE J. Transl. Eng. Health Med. *6*, 2100510. https://doi.org/10.1109/JTEHM.2018.2822681.
4. Bandodkar, A.J., Jeerapan, I., and Wang, J. (2016). Wearable Chemical Sensors: Present Challenges and Future Prospects. ACS Sens. *1*, 464–482. https://doi.org/10.1021/acssensors.6b00250.
5. Lu, Y., Fujita, Y., Honda, S., Yang, S.-H., Xuan, Y., Xu, K., Arie, T., Akita, S., and Takei, K. (2021). Wireless and Flexible Skin Moisture and Temperature Sensor Sheets toward the Study of Thermoregulator Center. Adv. Healthc. Mater. *10*, 2100103. https://doi.org/10.1002/adhm.202100103.
6. Park, B., Shin, J.H., Ok, J., Park, S., Jung, W., Jeong, C., Choy, S., Jo, Y.J., and Kim, T. (2022). Cuticular pad–inspired selective frequency damper for nearly dynamic noise–free bioelectronics. Science *376*, 624–629. https://doi.org/10.1126/science.abj9912.
7. Yu, X., Xie, Z., Yu, Y., Lee, J., Vazquez-Guardado, A., Luan, H., Ruban, J., Ning, X., Akhtar, A., Li, D., et al. (2019). Skin-integrated wireless haptic interfaces for virtual and augmented reality. Nature *575*, 473–479. https://doi.org/10.1038/s41586-019-1687-0.
8. Wang, M., Yang, Y., Min, J., Song, Y., Tu, J., Mukasa, D., Ye, C., Xu, C., Heflin, N., McCune, J.S., et al. (2022). A wearable electrochemical biosensor for the monitoring of metabolites and nutrients. Nat. Biomed. Eng. *6*, 1225–1235. https://doi.org/10.1038/s41551-022-00916-z.
9. Jiang, Y., Zhang, Z., Wang, Y.-X., Li, D., Coen, C.-T., Hwaun, E., Chen, G., Wu, H.-C., Zhong, D., Niu, S., et al. (2022). Topological supramolecular network enabled high-conductivity, stretchable organic bioelectronics. Science *375*, 1411–1417. https://doi.org/10.1126/science.abj7564.
10. Bariya, M., Li, L., Ghattamaneni, R., Ahn, C.H., Nyein, H.Y.Y., Tai, L.-C., and Javey, A. (2020). Glove-based sensors for multimodal monitoring of natural sweat. Sci. Adv. *6*, eabb8308. https://doi.org/10.1126/sciadv.abb8308.
11. Song, Y., Min, J., Yu, Y., Wang, H., Yang, Y., Zhang, H., and Gao, W. (2020). Wireless battery-free wearable sweat sensor powered by human motion. Sci. Adv. *6*, eaay9842. https://doi.org/10.1126/sciadv.aay9842.
12. Jiang, Z., Chen, N., Yi, Z., Zhong, J., Zhang, F., Ji, S., Liao, R., Wang, Y., Li, H., Liu, Z., et al. (2022). A 1.3-micrometre-thick elastic conductor for seamless on-skin and implantable sensors. Nat. Electron. *5*, 784–793. https://doi.org/10.1038/s41928-022-00868-x.
13. Luo, Y., Abidian, M.R., Ahn, J.-H., Akinwande, D., Andrews, A.M., Antonietti, M., Bao, Z., Berggren, M., Berkey, C.A., Bettinger, C.J., et al. (2023). Technology roadmap for flexible sensors. ACS Nano *17*, 5211–5295.
14. Ding, Y., Jiang, J., Wu, Y., Zhang, Y., Zhou, J., Zhang, Y., Huang, Q., and Zheng, Z. (2024). Porous Conductive Textiles for Wearable Electronics. Chem. Rev. *124*, 1535–1648. https://doi.org/10.1021/acs.chemrev.3c00507.
15. Gunawardhana, K.R.S., Wanasekara, N.D., Wijayantha, K.G., and Dharmasena, R.D.I. (2022). Scalable Textile Manufacturing Methods for Fabricating Triboelectric Nanogenerators with Balanced Electrical and Wearable Properties. ACS Appl. Electron. Mater. *4*, 678–688. https://doi.org/10.1021/acsaelm.1c01095.
16. Yu, Z., Deng, C., Seidi, F., Yong, Q., Lou, Z., Meng, L., Liu, J., Huang, C., Liu, Y., Wu, W., et al. (2022). Air-permeable and flexible multifunctional cellulose-based textiles for bio-protection, thermal heating conversion, and electromagnetic interference shielding. J. Mater. Chem. A Mater. *10*, 17452–17463. https://doi.org/10.1039/D2TA04706C.
17. Zhang, Y., Fu, J., Ding, Y., Babar, A.A., Song, X., Chen, F., Yu, X., and Zheng, Z. (2024). Thermal and Moisture Managing E-Textiles Enabled by Janus Hierarchical Gradient Honeycombs. Advanced Materials *n/a*. Adv. Mater. *36*, 2311633. https://doi.org/10.1002/adma.202311633.
18. Huang, Q., and Zheng, Z. (2022). Pathway to Developing Permeable Electronics. ACS Nano *16*, 15537–15544. https://doi.org/10.1021/acsnano.2c08091.
19. Shi, Y., Zhang, Z., Huang, Q., Lin, Y., and Zheng, Z. (2023). Wearable sweat biosensors on textiles for health monitoring. J. Semicond. *44*, 021601. https://doi.org/10.1088/1674-4926/44/2/021601.
20. Wang, P., Ma, X., Lin, Z., Chen, F., Chen, Z., Hu, H., Xu, H., Zhang, X., Shi, Y., Huang, Q., et al. (2024). Well-defined in-textile photolithography towards permeable textile electronics. Nat. Commun. *15*, 887. https://doi.org/10.1038/s41467-024-45287-y.
21. He, W., Wang, C., Wang, H., Jian, M., Lu, W., Liang, X., Zhang, X., Yang, F., and Zhang, Y. (2019). Integrated textile sensor patch for real-time and multiplex sweat analysis. Sci. Adv. *5*, eaax0649. https://doi.org/10.1126/sciadv.aax0649.
22. Terse-Thakoor, T., Punjiya, M., Matharu, Z., Lyu, B., Ahmad, M., Giles, G.E., Owyeung, R., Alaimo, F., Shojaei Baghini, M., Brunyé, T.T., and Sonkusale, S. (2020). Thread-based multiplexed sensor patch for real-time

sweat monitoring. npj Flex Electron *4*, 18. https://doi.org/10.1038/s41528-020-00081-w.

23. Wang, R., Zhai, Q., An, T., Gong, S., and Cheng, W. (2021). Stretchable gold fiber-based wearable textile electrochemical biosensor for lactate monitoring in sweat. Talanta *222*, 121484. https://doi.org/10.1016/j.talanta.2020.121484.
24. Zheng, L., Zhu, M., Wu, B., Li, Z., Sun, S., and Wu, P. (2021). Conductance-stable liquid metal sheath-core microfibers for stretchy smart fabrics and self-powered sensing. Sci. Adv. *7*, eabg4041. https://doi.org/10.1126/sciadv.abg4041.
25. Jeong, S.Y., Shim, H.R., Na, Y., Kang, K.S., Jeon, Y., Choi, S., Jeong, E.G., Park, Y.C., Cho, H.-E., Lee, J., et al. (2021). Foldable and washable textile-based OLEDs with a multi-functional near-room-temperature encapsulation layer for smart e-textiles. npj Flex Electron *5*, 15. https://doi.org/10.1038/s41528-021-00112-0.
26. Shak Sadi, M., and Kumpikaitė, E. (2022). Advances in the Robustness of Wearable Electronic Textiles: Strategies, Stability, Washability and Perspective. Nanomaterials *12*, 2039. https://doi.org/10.3390/nano12122039.
27. Yang, S., Liu, S., Ding, X., Zhu, B., Shi, J., Yang, B., Liu, S., Chen, W., and Tao, X. (2021). Permeable and washable electronics based on polyamide fibrous membrane for wearable applications. Compos. Sci. Technol. *207*, 108729. https://doi.org/10.1016/j.compscitech.2021.108729.
28. Thivya, P., Ramya, R., and Wilson, J. (2020). Poly(3,4-ethylenedioxythiophene)/taurine biocomposite on screen printed electrode: Non-enzymatic cholesterol biosensor. Microchem. J. *157*, 105037. https://doi.org/10.1016/j.microc.2020.105037.
29. Dhanjai, Lu, X., Wu, L., Chen, J., Lu, Y., and Lu, Y. (2020). Robust Single-Molecule Enzyme Nanocapsules for Biosensing with Significantly Improved Biosensor Stability. Anal. Chem. *92*, 5830–5837. https://doi.org/10.1021/acs.analchem.9b05466.
30. Hua, Q., and Shen, G. (2023). A wearable sweat patch for non-invasive and wireless monitoring inflammatory status. J. Semicond. *44*, 100401–100403. https://doi.org/10.1088/1674-4926/44/10/100401.
31. Camilleri, J., Borg, J., Damidot, D., Salvadori, E., Pilecki, P., Zaslansky, P., and Darvell, B.W. (2020). Colour and chemical stability of bismuth oxide in dental materials with solutions used in routine clinical practice. PLoS One *15*, e0240634. https://doi.org/10.1371/journal.pone.0240634.
32. Coomaraswamy, K.S., Lumley, P.J., Shelton, R.M., and Hofmann, M.P. (2007). Evaluation of Different Radiopacifiers for an MTA-Like Dental Cement. Key Eng. Mater. *361–363*, 885–888. https://doi.org/10.4028/www.scientific.net/KEM.361-363.885.
33. Coomaraswamy, K.S., Lumley, P.J., and Hofmann, M.P. (2007). Effect of Bismuth Oxide Radioopacifier Content on the Material Properties of an Endodontic Portland Cement–based (MTA-like) System. J. Endod. *33*, 295–298. https://doi.org/10.1016/j.joen.2006.11.018.
34. Chen, M.-S., Lin, H.-N., Cheng, Y.-C., Fang, A., Chen, C.-Y., Lee, P.-Y., and Lin, C.-K. (2020). Effects of Milling Time, Zirconia Addition, and Storage Environment on the Radiopacity Performance of Mechanically Milled Bi2O3/ZrO2 Composite Powders. Materials *13*, 563. https://doi.org/10.3390/ma13030563.
35. Yang, T.-S., Chen, M.-S., Huang, C.-J., Chen, C.-Y., Brangule, A., Zarkov, A., Kareiva, A., Lin, C.-K., and Yang, J.-C. (2021). A Novel Sol-Gel Bi2-xHfxO3+x/2 Radiopacifier for Mineral Trioxide Aggregates (MTA) as Dental Filling Materials. Appl. Sci. *11*, 7292. https://doi.org/10.3390/app11167292.
36. Gao, Y., Nolan, A.M., Du, P., Wu, Y., Yang, C., Chen, Q., Mo, Y., and Bo, S.-H. (2020). Classical and Emerging Characterization Techniques for Investigation of Ion Transport Mechanisms in Crystalline Fast Ionic Conductors. Chem. Rev. *120*, 5954–6008. https://doi.org/10.1021/acs.chemrev.9b00747.
37. Zhang, Z., and Nazar, L.F. (2022). Exploiting the paddle-wheel mechanism for the design of fast ion conductors. Nat. Rev. Mater. *7*, 389–405. https://doi.org/10.1038/s41578-021-00401-0.
38. Lin, Q., and Wang, L. (2023). Layered double hydroxides as electrode materials for flexible energy storage devices. J. Semicond. *44*, 041601. https://doi.org/10.1088/1674-4926/44/4/041601.
39. Mei, J., Liao, T., Ayoko, G.A., and Sun, Z. (2019). Two-Dimensional Bismuth Oxide Heterostructured Nanosheets for Lithium- and Sodium-Ion Storages. ACS Appl. Mater. Interfaces *11*, 28205–28212. https://doi.org/10.1021/acsami.9b09882.
40. Zhang, J., Dang, W., Yan, X., Li, M., Gao, H., and Ao, Z. (2014). Doping indium in β-Bi 2 O 3 to tune the electronic structure and improve the photocatalytic activities: first-principles calculations and experimental investigation. Phys. Chem. Chem. Phys. *16*, 23476–23482. https://doi.org/10.1039/C4CP02656J.
41. Cheng, H., Huang, B., Lu, J., Wang, Z., Xu, B., Qin, X., Zhang, X., and Dai, Y. (2010). Synergistic effect of crystal and electronic structures on the visible-light-driven photocatalytic performances of Bi2O3 polymorphs. Phys. Chem. Chem. Phys. *12*, 15468–15475. https://doi.org/10.1039/C0CP01189D.
42. Pereira, A.L.J., Sans, J.A., Vilaplana, R., Gomis, O., Manjón, F.J., Rodríguez-Hernández, P., Muñoz, A., Popescu, C., and Beltrán, A. (2014). Isostructural Second-Order Phase Transition of β-Bi2O3 at High Pressures: An Experimental and Theoretical Study. J. Phys. Chem. C *118*, 23189–23201. https://doi.org/10.1021/jp507826j.
43. Qiao, Y., Qiao, L., Chen, Z., Liu, B., Gao, L., and Zhang, L. (2022). Wearable Sensor for Continuous Sweat Biomarker Monitoring. Chemosensors *10*, 273. https://doi.org/10.3390/chemosensors10070273.
44. Anastasova, S., Crewther, B., Bembnowicz, P., Curto, V., Ip, H.M., Rosa, B., and Yang, G.-Z. (2017). A wearable multisensing patch for continuous sweat monitoring. Biosens. Bioelectron. *93*, 139–145. https://doi.org/10.1016/j.bios.2016.09.038.
45. McCaul, M., Porter, A., Barrett, R., White, P., Stroiescu, F., Wallace, G., and Diamond, D. (2018). Wearable Platform for Real-time Monitoring of Sodium in Sweat. ChemPhysChem *19*, 1531–1536. https://doi.org/10.1002/cphc.201701312.
46. Parrilla, M., Cuartero, M., Padrell Sánchez, S., Rajabi, M., Roxhed, N., Niklaus, F., and Crespo, G.A. (2019). Wearable All-Solid-State Potentiometric Microneedle Patch for Intradermal Potassium Detection. Anal. Chem. *91*, 1578–1586. https://doi.org/10.1021/acs.analchem.8b04877.
47. Montes-García, V., de Oliveira, R.F., Wang, Y., Berezin, A., Fanjul-Bolado, P., González García, M.B., Hermans, T.M., Bonifazi, D., Casalini, S., and Samorì, P. (2021). Harnessing Selectivity and Sensitivity in Ion Sensing via Supramolecular Recognition: A 3D Hybrid Gold Nanoparticle Network Chemiresistor. Adv. Funct. Mater. *31*, 2008554. https://doi.org/10.1002/adfm.202008554.
48. Manjakkal, L., Dervin, S., and Dahiya, R. (2020). Flexible potentiometric pH sensors for wearable systems. RSC Adv. *10*, 8594–8617. https://doi.org/10.1039/D0RA00016G.
49. Zhang, Y., Luo, Y., Wang, L., Ng, P.F., Hu, H., Chen, F., Huang, Q., and Zheng, Z. (2022). Destructive-Treatment-Free Rapid Polymer-Assisted Metal Deposition for Versatile Electronic Textiles. ACS Appl. Mater. Interfaces *14*, 56193–56202. https://doi.org/10.1021/acsami.2c19278.
50. Guo, R., Yu, Y., Xie, Z., Liu, X., Zhou, X., Gao, Y., Liu, Z., Zhou, F., Yang, Y., and Zheng, Z. (2013). Matrix-Assisted Catalytic Printing for the Fabrication of Multiscale, Flexible, Foldable, and Stretchable Metal Conductors. Adv. Mater. *25*, 3343–3350. https://doi.org/10.1002/adma.201301184.
51. Yu, Y., Yan, C., and Zheng, Z. (2014). Polymer-Assisted Metal Deposition (PAMD): A Full-Solution Strategy for Flexible, Stretchable, Compressible, and Wearable Metal Conductors. Adv. Mater. *26*, 5508–5516. https://doi.org/10.1002/adma.201305558.
52. Li, P., Zhang, Y., and Zheng, Z. (2019). Polymer-Assisted Metal Deposition (PAMD) for Flexible and Wearable Electronics: Principle, Materials, Printing, and Devices. Adv. Mater. *31*, 1902987. https://doi.org/10.1002/adma.201902987.

53. Lin, Y., Bariya, M., Nyein, H.Y.Y., Kivimäki, L., Uusitalo, S., Jansson, E., Ji, W., Yuan, Z., Happonen, T., Liedert, C., et al. (2019). Porous Enzymatic Membrane for Nanotextured Glucose Sweat Sensors with High Stability toward Reliable Noninvasive Health Monitoring. Adv. Funct. Mater. *29*, 1902521. https://doi.org/10.1002/adfm.201902521.

54. Yu, Y., Nassar, J., Xu, C., Min, J., Yang, Y., Dai, A., Doshi, R., Huang, A., Song, Y., Gehlhar, R., et al. (2020). Biofuel-powered soft electronic skin with multiplexed and wireless sensing for human-machine interfaces. Sci. Robot. *5*, eaaz7946. https://doi.org/10.1126/scirobotics.aaz7946.

55. Wang, Z., Shin, J., Park, J.-H., Lee, H., Kim, D.-H., and Liu, H. (2021). Engineering Materials for Electrochemical Sweat Sensing. Adv. Funct. Mater. *31*, 2008130. https://doi.org/10.1002/adfm.202008130.

56. Huang, C.-C., Wen, T.-Y., and Fung, K.-Z. (2006). Orientation-controlled phase transformation of Bi2O3 during oxidation of electrodeposited Bi film. Mater. Res. Bull. *41*, 110–118. https://doi.org/10.1016/j.materresbull.2005.07.043.

57. Chen, X., Li, Y., Yang, Y., Zhang, D., Guan, Y., Bao, M., and Wang, Z. (2022). A super-hydrophobic and antibiofouling membrane constructed from carbon sphere-welded MnO2 nanowires for ultra-fast separation of emulsion. J. Membr. Sci. *653*, 120514. https://doi.org/10.1016/j.memsci.2022.120514.

58. Liu, Y., Yang, W., Zhang, P., and Zhang, J. (2018). Nitric acid-treated birnessite-type MnO2: An efficient and hydrophobic material for humid ozone decomposition. Appl. Surf. Sci. *442*, 640–649. https://doi.org/10.1016/j.apsusc.2018.02.204.

59. Merachtsaki, D., Tsardaka, E.-C., Anastasiou, E., and Zouboulis, A. (2021). Anti-corrosion properties of magnesium oxide/magnesium hydroxide coatings for application on concrete surfaces (sewerage network pipes). Construct. Build. Mater. *312*, 125441. https://doi.org/10.1016/j.conbuildmat.2021.125441.

60. Yin, S., Yang, H., Dong, Y., Qu, C., Liu, J., Guo, T., and Duan, K. (2021). Environmentally favorable magnesium phosphate anti-corrosive coating on carbon steel and protective mechanisms. Sci. Rep. *11*, 197. https://doi.org/10.1038/s41598-020-79613-3.

61. Younis, A.A., El-Sabbah, M.M.B., and Holze, R. (2012). The effect of chloride concentration and pH on pitting corrosion of AA7075 aluminum alloy coated with phenyltrimethoxysilane. J. Solid State Electrochem. *16*, 1033–1040. https://doi.org/10.1007/s10008-011-1476-7.